Cellulose
https://doi.org/10.1007/s10570-021-04384-7

ORIGINAL RESEARCH

Printable, castable, nanocrystalline cellulose-epoxy composites exhibiting hierarchical nacre-like toughening

Abhinav Rao · Thibaut Divoux · Crystal E. Owens · A. John Hart

Received: 26 August 2021 / Accepted: 16 December 2021
© The Author(s), under exclusive licence to Springer Nature B.V. 2022

Abstract Due to their exceptional mechanical and chemical properties and their natural abundance, cellulose nanocrystals (CNCs) are promising building blocks of sustainable polymer composites. However, the rapid gelation of CNC dispersions has generally limited CNC-based composites to low CNC fractions, in which polymer remains the dominant phase. Here we report on the formulation and processing of crosslinked CNC-epoxy composites with a CNC fraction exceeding 50 wt%. The microstructure comprises sub-micrometer aggregates of CNCs crosslinked to polymer, which is analogous to the lamellar structure of nacre and promotes toughening mechanisms associated with bulk ductility, despite the brittle behavior of the aggregates at the nanoscale. At 63 wt% CNCs, the composites exhibit a hardness of 0.66 GPa and a fracture toughness of 5.2 MPa $m^{1/2}$. The hardness of this all-organic material is comparable to aluminum alloys, and the fracture toughness at the centimeter scale is comparable to that of wood cell walls. We show that 3D CNC-epoxy composite objects can be shaped from the gel precursors by direct-write printing, casting, and machining. The formulation, processing route, and insights on toughening mechanisms gained from our multiscale approach can be applied broadly to highly loaded nanocomposites.

Keywords Cellulose · Composites · Nacre · Wood · Structural materials · Mechanics · Additive manufacturing · Sustainable

Supplementary Information The online version contains supplementary material available at https://doi.org/10.1007/s10570-021-04384-7.

A. Rao (✉) · C. E. Owens · A. J. Hart
Department of Mechanical Engineering, Massachusetts Institute of Technology, Cambridge, MA 02139, USA
e-mail: raoa@mit.edu

A. J. Hart
e-mail: ajhart@mit.edu

T. Divoux
MultiScale Material Science for Energy and Environment, UMI 3466 CNRS-MIT, 77 Massachusetts Avenue, Cambridge, Massachusetts 02139, USA

T. Divoux
Univ Lyon, Ens de Lyon, Univ Claude Bernard, CNRS, Laboratoire de Physique, University of Lyon, 69342 Lyon, France

Introduction

Cellulose is nature's most abundant polymer, and an estimated 10^{10} to 10^{11} tons of cellulose are synthesized and naturally degraded each year (Zhao et al. 2007). Cellulose nanocrystals (CNCs), which can be extracted from natural cellulose fibers by acid hydrolysis (Lagerwall et al. 2014; Habibi et al. 2010), are of growing interest as ingredients in the production of

Published online: 10 February 2022

sustainable composites due to their attractive mechanical properties, including an axial Young's modulus of 150 GPa, and their sustainability and biocompatibility (Moon et al. 2011; Hon 1994; Kim et al. 2015).

Processing CNC composites with uniform dispersion and strong bonding between CNCs and polymers remains challenging because suspensions of CNCs are susceptible to gelation and phase separation at relatively low concentrations (Klemm et al. 2011; George and Sabapathi 2015). Previous studies have shown that CNCs reinforce polymer films resulting in improved mechanical properties and thermal stability (Khelifa et al. 2016; Pruksawan et al. 2020; Siqueira et al. 2017). Yet, there remains an opportunity to further analyze the multiscale relationships between processing, microstructure, and mechanical properties of CNC-polymer composites.

More broadly, naturally occurring nanocomposites provide compelling inspiration for the design of new synthetic materials. For instance, the high specific strength and toughness of wood originate from the architecture of its cell walls (Wegst et al. 2015; Barthelat et al. 2016; Adler and Buehler 2013), which comprise parallel filaments of cellulose linked by a matrix of hemicellulose and lignin arranged in layers with micro-scale thickness. Mineral-based nanocomposites such as nacre, enamel, and bone achieve high strength and toughness via optimized microstructures that enable hierarchical damage resistance (Ritchie 2011; Dunlop and Fratzl 2010; Dunlop et al. 2011; Pro and Barthelat 2019; Wegst et al. 2015), such as the brick and mortar microstructure of nacre (Gu et al. 2017). Therein, stiff, brittle platelets are arranged in a lamellar structure, linked together with a small volume fraction of a relatively soft polymeric interfacial material. Nacre-inspired composites have been synthesized using a variety of platelet materials, including graphene, ceramics, and rigid polymers, with dimensions spanning from nanometers to millimeters in length (Li et al. 2012; Zhao et al. 2018; Le Ferrand et al. 2015; Gao et al. 2017; Wang and Shaw 2009; Gu et al. 2017). In general, the irregular interfaces in these composites promote fracture toughening mechanisms such as crack deflection, bridging, and branching, which result in a high fracture toughness without significantly compromising the stiffness and strength provided by the individual platelets. In addition, the nacre-like microstructure can confer a ductile behavior to conventionally brittle materials, such as ceramics (Bouville et al. 2014).

Here, we report on the formulation, mechanical properties, and near-net-shape fabrication of strong and tough CNC-epoxy composites with CNC loading exceeding 50% wt. A gel precursor comprising CNCs and epoxide oligomers dispersed in a solvent is printed by direct ink writing and crosslinked to form dry, solid CNC-epoxy nanocomposites. The gel-based approach allows viscous flow necessary for printing and near-net-shape molding and results in a high CNC loading in the composite. The resulting composites are characterized mechanically at multiple length scales using a combination of atomic force microscopy (AFM), nanoindentation, microindentation, and scratch tests. We show that the composites display a nanoscale granular structure resembling the brick and mortar architecture of nacre, where the grain size plays a key role in determining the mechanical properties of the composite. Notably, the micro-mechanical response of the composite resembles that of a ductile material, despite an inherently brittle behavior at the nanoscale. While similar effects have been observed for composites with inorganic fillers, we use multiscale mechanical testing to demonstrate the influence of CNC chemistry and processing in determining the behavior of the composite. At the microscale, we observe that the toughening is a consequence of fracture toughening mechanisms such as crack branching, bridging, and deflection.

Experimental

Materials

UV curable CNC gels (UV-CG) were prepared by first dissolving an epoxide oligomer, a photoinitiator, and a thermal crosslinker in dimethylformamide (DMF). The oligomer is poly(bisphenol-a-co-epichlorohydrin) diglycidyl ether ($M_n \sim 355$ g/mol), the cationic photoinitiator is triarylsulfonium hexafluorophosphate (50% in propylene carbonate) and the thermal crosslinker is 4-aminophenyl sulfone. All reagents were obtained from Sigma Aldrich. Freeze-dried CNC powder (Cellulose Lab, New Brunswick, Canada) is added to the mixture and then dispersed by probe sonication at 40% amplitude for 15 seconds (750 W Sonics Vibra Cell). Reference *composite gels* (CG)

were prepared using the same process, without adding the photoinitiator nor the thermal crosslinker. In all the gels, the mass ratio of the epoxide oligomer to the CNCs is 10%, and the mass of the cationic photoinitiator is 10% of the mass of the epoxide oligomer. The amine to epoxide molar ratio is 0.4. The mass fractions of the crosslinkers are selected to allow UV curing of millimeter-thick layers within a few minutes and accelerated thermal curing at lower temperatures.

Printing

The samples are printed using a custom direct-ink writing printer based on a Hyrel 3D Engine SR printer. A pneumatic extruder (Nordson 184 HP7x) is mounted to the printer. The pump (Nordson Ultra 2400) is driven by an integrated relay on the printer. The gel expands slightly upon extrusion, and the thickness of each layer is approximately 0.5 mm. UV-curable gels are partially cured under a UV flood lamp (Dymax 2000-EC) for 5 minutes. Following this, they still contain solvent but have higher mechanical integrity. Aside from this step, the curing process is identical for both UV and thermally curable samples. The sample is then air-dried to remove a majority of the solvent. A two-stage thermal cure - first at 80°C for 6 hours and 130°C for 4 hours is used to fully harden the samples. The printed samples are then polished on a rotary polisher using a silicon carbide polishing paper of grit P4000 (Buehler) prior to any mechanical testing. The thickness of the cured samples was around 1 mm, around 100 times the largest indentation depth.

Imaging and mechanical characterization

Atomic Force Microscopy (AFM) images were obtained using a Cypher S AFM (Asylum Research). Statistical nanoindentation tests were conducted on a Hysitron Triboindenter equipped with a three-sided pyramid diamond Berkovich indenter. A 3-step trapezoidal load profile consists of loading and unloading steps of 10 s each, separated by a 5 s hold at the desired peak load. The hold allows viscoelastic relaxation to occur prior to the unloading step, during which hardness and modulus are measured, using the Oliver-Pharr method (Oliver and Pharr 1992). Statistical analysis of nanoindentation data and image processing for grain size measurement is described in sections 2-4 of the supplementary information. The scratch and microindentation experiments were performed using a Rockwell indenter connected to a Micro Combi Tester (Anton Paar). During scratch tests, the vertical load on the indenter was increased linearly from 30 mN to 30 N over a scratch length of 3 mm. The samples were mounted on steel substrates for indentation and scratch testing.

Micromilling

Bulk CNC artifacts were fabricated by micromilling (Roland SRM-20) a block of the composite. The composite was formed by molding the material into a 10 cm × 5 cm × 5 cm volume and thermally curing. Cutting parameters for a 0.0190" diameter square endmill were 9500 revolutions per minute and feed of 270 mm min^{-1}.

Results and Discussion

The printing and curing sequence to produce near-net-shape composites is shown in Fig. 1a. To fabricate composite solids, first, the gel is extruded from the nozzle of a 3D printer at constant pressure P, while the print bed moves at a print speed v relative to the extruder. The geometry of the nozzle and the print speed determine the shear rate and total shear strain imposed on the gel during this process. The shear deformation of the gel results in partial and yet irreversible degradation of the network of hydrogen bonds connecting the CNCs, thus allowing the gel to flow (Rao et al. 2019). However, by selecting a suitably high CNC concentration, the gel retains its shape after extrusion. Upon curing, the hydroxyl groups on the CNCs form covalent crosslinks with the epoxide monomers via a ring-opening mechanism (Khelifa et al. 2016). A photograph of the printing apparatus is shown in Fig. 1b, and further details on gel formulation and printing are provided in supplementary Fig. S1. Around 12 mL of gel is necessary to print a 2.5 cm^3 sample, with an estimated volumetric shrinkage of around 80%. A majority of the shrinkage occurs during the initial drying process, and is associated with solvent evaporation. By using a physical gel, phase-separation is minimized as the CNCs are constrained by hydrogen bonds. The strength of the gel also permits the printed traces to

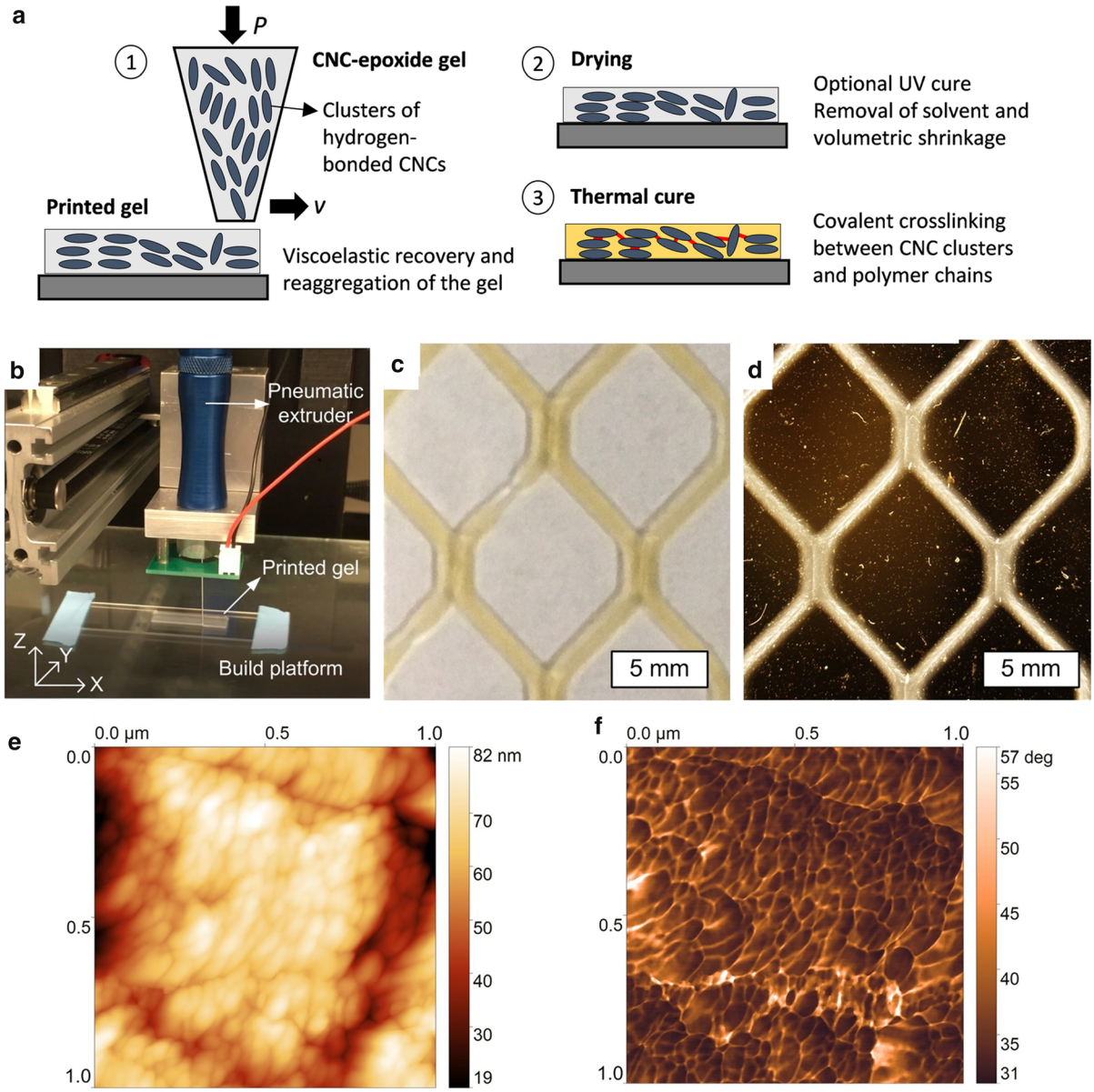

Fig. 1 Fabrication of CNC-epoxy composites: **a** Schematic showing the microstructure of the gel precursor during printing and post-cure processing sequence. The gel is initially composed of locally aligned CNC domains, within which the CNCs are linked by hydrogen bonds. These hydrogen bonds are partially broken during shear flow imposed by extrusion. After printing, the gel is dried and thermally cured to produce the final, dense composite. **b** The 3D printer with a numerically controlled pneumatic extruder and a heated print bed. **c** Bright light and **d** Cross-polarized optical microscope image of the CNC-epoxide composite printed in a hexagonal lattice pattern showing bright nematic domains and good shape retention of the traces **e**, **f** AFM topography and phase images (1 μm^2 area), respectively, reveal that the printed composites have a granular microstructure, with grain size of around 100 nm

retain their geometry. Between the drying and thermal cure steps, the gel may be molded or embossed, with minimal shrinkage thereafter.

The shear history applied during the extrusion process plays a key role in regulating the grain size in the composite. Moreover, controlling the layer thickness is important to limit shrinkage stresses and the

formation of macroscopic defects during solvent evaporation from the gel. Thus, additive manufacturing is a desirable process for synthesizing bulk composites from gel precursors and potentially enables control of the micro- and macro-structure of the composite. Herein, we refer to the CNC gels as "CG". We also discuss the processing of a UV-curable gel, denoted "UV-CG", which is identical to the CGs, except for the addition of a photoinitiator, which promotes the same crosslinking mechanism between CNCs and epoxide upon UV exposure. Both the CG and UV-CG were printed using the direct-write process. Yet the UV-CG is exposed to ultraviolet light after printing, followed by heating to complete crosslinking (see supplementary information section 1).

The process of dispersion of CNCs in the gel is critical to avoid precipitation of large aggregates of CNCs and phase separation. In the present work, a probe sonicator is used to disperse CNCs in the solvent. The sonication process was optimized for sample volumes of around 10 mL. Furthermore, printing samples beyond the centimeter scale requires an enclosed print chamber to control solvent evaporation and a large-volume pneumatic extruder to print a larger volume of gels. While these limitations preclude large-scale mechanical testing, we comprehensively study the structure-property relationships from nanometer to millimeter scale, capturing the interactions between clusters of a few CNCs and relating it to the "composite" behavior of the bulk material. The methods of micro-hardness and fracture toughness testing applied here are routinely used to characterize materials with volume-dependent heterogeneity (Borodich et al. 2015). These methods can serve as useful approximations of conventional engineering tests, while providing valuable microstructural insights for materials with multiple length scales (Akono et al. 2011, 2012; Randall et al. 2009).

A preliminary examination of the CNC-epoxide composite, by comparing the optical and cross-polarized images, shows the presence of nematic domains of CNCs (Fig. 1c and d). The bright colors in the cross-polarized images have been widely used to identify nematic liquid crystals formed in CNC suspensions (Abitbol and Cranston 2014; Schütz et al. 2015; Gray and Mu 2015). AFM amplitude and phase images within these domains, reveal an anisotropic, nanoscale grain structure of typical size 100 nm, as shown in Fig. 1e and f respectively. As observed in the amplitude image, the grain orientation indicates a local order corresponding to the direction of extrusion. Furthermore, upon comparing the amplitude and phase images, we find that the phase recorded for the grains is relatively constant, regardless of the topographical variations across the scanned region. However, the grain boundaries remain distinct in phase throughout the image. This observation suggests that the composition and mechanical properties of the grain boundaries are distinct from those of the grains.

Such a distinction is due to the microstructure of the gel and how it evolves during processing. The CNC-polymer gels possess a glassy microstructure composed of densely packed clusters made of CNCs linked by hydrogen bonds (Rao et al. 2019). These clusters are partially broken down during printing, as the shear flow irreversibly breaks hydrogen bonds. Once the gel is brought to rest, the clusters are rearranged by van der Waals attraction and by electrostatic repulsion between the CNCs, due to their native negative surface charge (Moon et al. 2011). As a result, the composite contains residual clusters forming larger grains, as well as freely dispersed individual CNCs surrounded by the epoxide monomer, as shown in Fig. 1d. The extent to which the shear flow disrupts the initial gel microstructure depends on the total shear strain applied during extrusion (Rao et al. 2019).

The local Young modulus of the composite is directly related to the strength of the intermolecular interactions at the CNC-CNC and CNC-polymer interfaces. Bimodal AFM imaging shows a modulus of 50 GPa at the grain boundaries and 30 GPa within the grains (see supplementary Fig. S2). The grains are composed of tightly packed and hydrogen-bonded CNCs and are likely to be infiltrated to a lower degree by the monomer, particularly as they persist during extrusion. As a result, the grains may have a lower degree of covalent crosslinking than the grain boundaries and thus a lower modulus.

The cumulative grain size distributions of the thermally cured (CG) and UV cured (UV-CG) composites were determined using AFM images of three regions on each sample (see supplementary Figs. S3, S4, and Table S1). We find a significant difference in grain size distributions for composites prepared from gels with (UV-CG) and without (CG) the photoinitiator, despite having the same CNC concentration. In the UV-cured gels, the photoinitiator has the effect of

screening the surface charges on the CNCs, promoting aggregation and grain growth (Rao et al. 2019). As a result, UV-cured composites have a larger average grain size with broader distribution, including grains larger than 200 nm. In contrast, thermally-cured composites have a narrow grain size distribution with an average size around 100 nm (Fig. 2a). The indentation modulus (or reduced modulus) E_r and hardness H of the composites were obtained by nanoindentation, and data is shown in Fig. 2b and c, respectively. Nanoindentation grids, consisting of 12×12 = 144 indents, were performed on each sample to a typical depth of 1 μm, corresponding to a peak load of 10 mN (see supplementary Fig. S5 and corresponding text for further discussion on the nanoindentation data analysis). The thermally-cured composite has distinctly better mechanical properties than the UV-cured composite, ($E_r = 9.2$ GPa vs. 7.3 GPa, and $H = 0.64$ GPa vs. 0.44 GPa, respectively).

The broader grain size distribution of UV-cured composites suggests that grain growth during the printing and curing processes must be controlled to achieve improved mechanical properties. To illustrate this point, we compare indentations performed with AFM tips in two representative locations of a UV-cured composite (Fig. 2d). Location (1) is chosen in a region with grains larger than 200 nm, whereas location (2) is picked in a region with smaller grains. The indents performed in these two regions are visible in Fig. 2e. Both indents were force-controlled, with a peak load of 0.5 μN. In region (1), the cracks emanating from the vertices of the indent are observed to propagate along the grain boundaries, resulting in the brittle fracture of the composite over a length scale

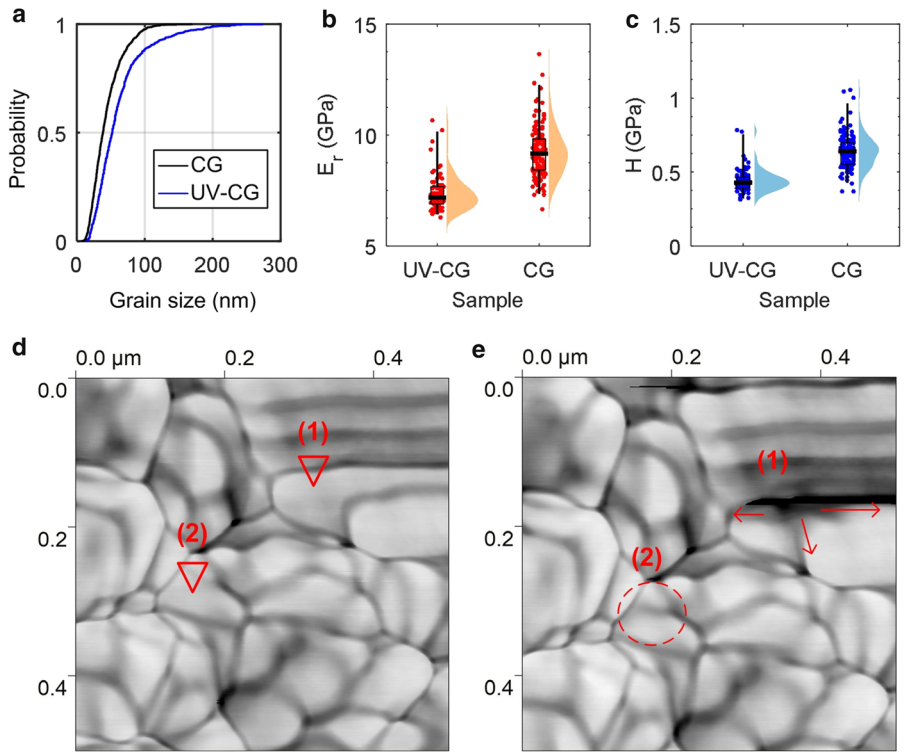

Fig. 2 Influence of grain size on micromechanical properties of CNC-epoxy composites: **a** Cumulative distribution of grain sizes in UV-cured composites (UV–CG) and thermally cured composites, without crosslinkers (CG). **b** Indentation modulus E_r and **c** Hardness H determined by nanoindentation, with 63% wt. CNCs in both cases. Data are presented as a "raincloud" plot (Allen et al. 2018); the box represents one standard deviation above and below the mean, and the whiskers represents the 75% confidence interval. Each data point represents an indent at a distinct location on the sample. **d** AFM images of a UV-cured composite (UV–CG) showing highly variable grain sizes. The triangles mark the locations where two indentation tests were performed, indicating large (1) and small (2) grains, respectively. **e** Image of the same region after indentation, showing that the indent in location (1) has triggered a crack larger than 150 nm at the interface between two adjacent grains, whereas the indent in location (2) had a localized impact (crack length <50 nm)

greater than 150 nm. By contrast, the plastic deformation in region (2) is confined to a region smaller than 100 nm in diameter, and the grain boundaries restrict the extent of the corresponding crack. Therefore, a narrow grain size distribution with a small average grain size is ideal for improving resistance to long-range crack propagation. We systematically varied the CNC mass fraction, finding that a CNC content of about 63% wt. corresponds to the maximum values of indentation modulus and hardness (see supplementary Fig. S6). The emergence of an optimum concentration may be attributed to the fact that a sufficient amount of polymer is necessary to surround and crosslink the CNCs to one another. Indeed, at higher CNC concentrations, the crosslink density is low, and the composite is more brittle, hence less resistant to plastic deformation. By contrast, at lower CNC concentrations, the CNCs contribute less to the composite modulus.

At this point, we can draw an analogy between the microstructure and mechanics of CNC-epoxy composites and those of biological composites such as bone and nacre, which are largely composed of brittle constituents, and yet display ductile mechanical behavior at larger scales (Barthelat et al. 2016). Here, statistical results from nanoindentation can connect the nanoscale mechanical behavior to the micromechanical properties of the CNC-epoxy composites, by relating the indentation depth to the intrinsic length scale of the microstructure of the material (Kushch et al. 2015). Indentation at shallow depth allows individual phases in the sample microstructure to be resolved, while deep indents provide averaged values representative of the macroscopic mechanical properties. We performed grids of 144 indents on a composite with 63% wt. CNCs, at peak loads, $P_{\max}$ from 0.1 mN to 1000 mN, which correspond to average indentation depths, $h_{\max}$ ranging from (74 ± 11) nm to (9349 ± 355) nm respectively. The values of E_{r} and H are reported as a function of both $P_{\max}$ and $h_{\max}$ in Fig. 3a and 3b respectively. For the chosen (Berkovich) indenter geometry, the length scale of the sample probed by an indent of depth $h_{\max}$ is approximately $3h_{\max}$ (Constantinides et al. 2006). Both the indentation modulus and the hardness of the CNC composites are observed to be independent of depth from the nanoscale to the microscale, with averaged values of $\bar{E}_{\mathrm{r}} = 10.3$ GPa and $\bar{H} = 0.66$ GPa respectively. The Young modulus can be calculated using the indentation modulus and Poisson's ratio (Oliver and Pharr 1992), here giving $E = 8.5$ GPa.

In general, the measured hardness increases with decreasing indentation depths due to the effect of discrete dislocations and surface roughness, and converges to the intrinsic hardness of the material at sufficiently large indentation depths. For heterogeneous materials, large indentation depths may be necessary to probe the "composite" properties rather than those of individual phases (Pharr et al. 2010; Shell De Guzman et al. 1993; Miller et al. 2008). For the CNC-epoxy composites, we observe that the hardness and elastic modulus measured over indentation depths spanning from around 100 nm to 1 μm are comparable (Fig. 3b). Therefore, we can conclude that a volume with a critical dimension of around 100 nm, comprising a few grains and their associated interfaces, is a representative element of the composite. The constant hardness of the CNC-epoxy composites versus indentation depth illustrates that toughening mechanisms enabled by the CNCs are hierarchical and contribute to improving the mechanical properties of the material at length scales that are several orders of magnitude larger than the CNC particles.

We now turn to the analysis of the plastic deformation after microindentation, along with scratch testing, to further quantify the fracture resistance of CNC-epoxy composites. A conical indenter is moved at constant speed across the surface of the sample while steadily increasing the vertical load and recording the tangential force F_T exerted on the indenter. Once normalized by the contact area, F_T converges, for large enough penetration depth of the indenter, towards the fracture toughness; prior studies show this matches the plane strain fracture toughness from conventional 3-point bending tests on notched samples (Akono et al. 2011; Akono and Ulm 2014). Both microindentation and scratch tests generate fracture patterns in the sample over micron to millimeter length scales. In Fig. 3c we show the residual plastic deformation from microindentation at a peak load of 10 mN. We note the absence of linear cracks emanating from the indent's vertices, indicating that the composite plastic behavior is ductile, rather than brittle (Skrzypczak et al. 2009). Moreover, the absence of linear cracks is also consistent with the amorphous microstructure of the composites (Cook and Pharr 1990). Figure 3d shows the plastic damage

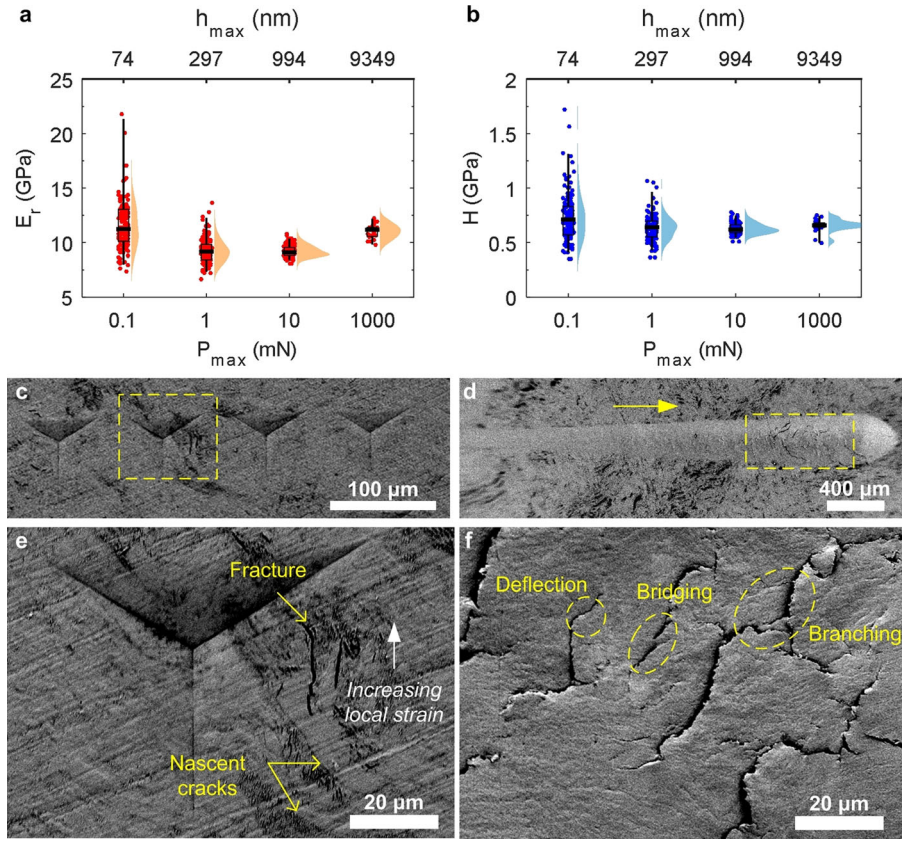

Fig. 3 Multiscale mechanical properties of thermally-cured CNC composites (CG) with 63% wt. CNCs: **a** Elastic modulus and **b** Hardness measured by nanoindentation at different peak loads ranging between 0.1 mN and 1 N. The corresponding average indentation depths range from 74 nm to 10 μm. For each set of data, the box plot indicates the mean, 75% confidence intervals, and maximum range of the data. **c** SEM image showing the plastic deformation due to an indent at a peak load of 1000 mN, **d** Plastic deformation resulting from a scratch test performed under increasing normal load from 30 mN to 3 N. The arrow indicates the scratch direction. High magnification images of the **e** indent and **f** scratch showing brittle plasticity at the microscale, and the fracture toughening mechanism contributing to bulk ductility

observed after a scratch test, wherein the arrow indicates the direction of the scratch test. The vertical load during the scratch test is increased linearly from 30 mN to 30 N along the scratch direction. For loads larger than 28 N, we observe cracks perpendicular to the scratch direction. This pattern of damage together and the absence of parabolic crack patterns at low vertical loads are characteristic of ductile polymers (Jiang et al. 2009). From the scratch load versus depth (Supplementary Fig. S7), we estimate a fracture toughness of 5.2 MPa.m$^{1/2}$ for a composite with 63% wt. CNCs.

High magnification images for the indent and the scratch shown in Fig. 3e and f, respectively, indicate that cracks originate from the regions subjected to large strains around the indenter. These cracks ultimately grow and branch into larger cracks, causing microscale fractures. The fracture path is not continuous, indicating that fracture energy is distributed by crack deflection and the splitting of cracks into multiple separate segments. Examination of the sample after the scratch test suggests that the crack propagation mechanisms are observed over longer length scales compared with those in the indent (Fig. 3f). In addition to being deflected, the propagation of long individual cracks is interrupted by branching and bridging. In the latter case, a bridge of material splits the crack into multiple regions. The crack geometry and propagation are analogous to that observed for nacre (Bouville et al. 2014; Gao et al. 2017; Niebel et al. 2016), and are a direct consequence of the deflection and arrest of cracks by the glassy,

nanoscale grain structure of the CNC-epoxy composites. The fracture energy is dissipated at the grain boundaries due to the high crosslink density and the discontinuous arrangement of the grains.

Our results show that the micromechanical properties of the CNC-epoxy composites exceed those of many engineering polymers and all-organic materials, and that they are comparable to those of wood cell wall. (Fig. 4a) (Ashby 2011; Gao et al. 2017; Shen et al. 2004; Paplham et al. 1995; Tze et al. 2007; Briscoe et al. 1998; Song et al. 2018; Lichtenegger 2002; Imbeni et al. 2005; Staines et al. 1981). The reported modulus and hardness of nacre vary significantly based on source (Barthelat et al. 2006; Song et al. 2015; Bruet et al. 2005). While the predominantly inorganic phase of nacre results in a higher stiffness, the hardness of the CNC-epoxy composites is comparable to certain species of nacre. Notably, we observe these mechanical properties over length scales from 10 to 10^3 times the diameter of the CNCs. In comparison, wood, which is the source of CNCs, has a hierarchical structure wherein the microscale cell walls comprise layers of aligned cellulose microfibrils, interconnected by cellulose nanofibrils (Moon et al. 2011; Kretschmann 2003). Due to its macroscale cellular structure, the modulus and hardness of wood measured by microindentation are significantly lower than those measured by nanoindentation (Moon et al. 2009). Indeed, the hardness of a wood cell wall measured by nanoindentation is around 0.4 GPa, whereas the bulk hardness of wood, measured at depths up to 500 μm, ranges between 60 and 90 MPa.

Printed CNC-epoxy composites can also be further processed into macroscale objects having complex shapes. Here we demonstrate the fabrication of a model of a tooth, a potentially compelling application for a hard and tough biocomposite, by molding and curing a block of the (CG) CNC gel (Fig. 4b), followed by micromilling. The machined model of a tooth, shown in Fig. 4c illustrates that the bulk stiffness and the ductility of the CNC-epoxy composite enable machining of complex surface contours. The inset image shows tool marks from machining.

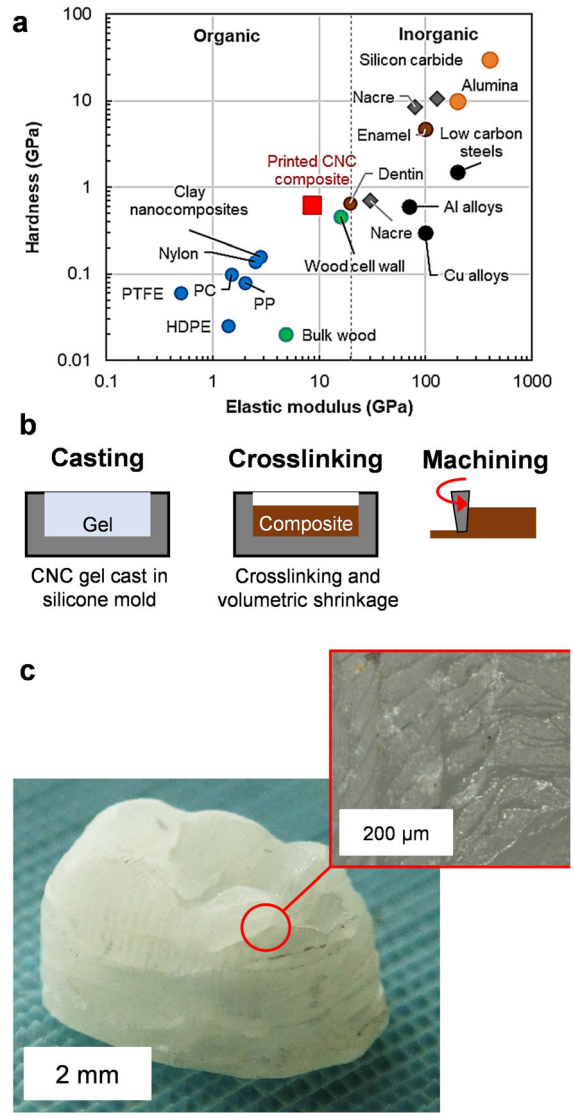

Fig. 4 Mechanical properties of the printed CNC composites in comparison with those of natural and synthetic materials: (Ashby 2011; Gao et al. 2017; Shen et al. 2004; Paplham et al. 1995; Tze et al. 2007; Briscoe et al. 1998; Song et al. 2018; Lichtenegger 2002; Imbeni et al. 2005; Staines et al. 1981; Tesch et al. 2001; Song et al. 2015; Barthelat et al. 2006; Bruet et al. 2005) **a** Average values of elastic modulus versus hardness determined by nanoindentation and **b** Fabrication sequence for a micromachined composite parts **c** Model of a tooth machined from a block of CNC-epoxide composite, with inset showing machined surface

Conclusion

We have demonstrated the processing and multi-scale mechanics of CNC-epoxy composites with high CNC mass fractions derived from versatile gel-based precursors. These composites comprise grains of aggregated CNCs that are crosslinked by covalent bonding. The tortuous paths formed by the grain boundaries resist the linear propagation of cracks between grains. The bridging, deflection, and branching of cracks impart macroscale toughness to the CNC-epoxy composites. The stiffness, hardness, and fracture toughness of the CNC composites exceed those of many engineering polymers. The composite response is ductile despite the inherently brittle behavior of the CNC grains. Our findings suggest that the addition of significant fractions of CNCs to petroleum-based polymers can potentially improve the mechanical properties and reduce the environmental impact of these ubiquitous materials. The fracture toughening mechanisms observed in these composites, as well as the relationships established between synthesis and microstructure, are more broadly applicable to molding and additive manufacturing of other nanocrystalline-polymer composites.

Acknowledgments The authors thank Sooraj Narayan and Prof. Lallit Anand for assistance with the finite element model. Financial support was provided by the Procter and Gamble Corporation, and we thank Neville Sonnenberg for discussions related to the project. C.E.O. was supported by the United States Department of Defense (DoD) through the National Defense Science & Engineering Graduate Fellowship (NDSEG) Program.

Author Contributions AR and AJH conceived and designed the project, AR designed and performed the experiments and interpreted the data, TD supported the experiments and contributed to data interpretation, CEO designed the tooth model and performed the micromilling experiments. AJH supervised the research. AR, TD and AJH wrote the manuscript. All authors discussed the results and reviewed the manuscript.

Funding Financial support was provided by the Procter and Gamble Corporation. C.E.O. was supported by the United States Department of Defense (DoD) through the National Defense Science & Engineering Graduate Fellowship (NDSEG) Program.

Declarations

Conflict of interests The authors declare that they have no conflicts of interest.

References

Abitbol T, Cranston ED (2014) Chiral nematic self-assembly of cellulose nanocrystals in suspensions and solid films. In: Handbook of green materials, world scientific, pp 37–56. https://doi.org/10.1142/9789814566469_0035

Adler DC, Buehler MJ (2013) Mesoscale mechanics of wood cell walls under axial strain. Soft Matter 9(29):7138. https://doi.org/10.1039/c3sm50183c

Akono AT, Ulm FJ (2014) An improved technique for characterizing the fracture toughness via scratch test experiments. Wear 313(1–2):117–124. https://doi.org/10.1016/j.wear.2014.02.015

Akono AT, Reis PM, Ulm FJ (2011) Scratching as a fracture process: from butter to steel. Phys Rev Lett 106(20):204302. https://doi.org/10.1103/PhysRevLett.106.204302

Akono AT, Randall NX, Ulm FJ (2012) Experimental determination of the fracture toughness via microscratch tests: application to polymers, ceramics, and metals. J Mater Res 27(02):485–493. https://doi.org/10.1557/jmr.2011.402

Allen M, Poggiali D, Whitaker K, Marshall TR, Kievit R (2018) Raincloud plots: a multi-platform tool for robust data visualization. Peer J 6:e27137v1 (Preprints). https://doi.org/10.7287/peerj.preprints.27137v1

Ashby MF (2011) Material property charts. In: Materials selection in mechanical design. Butterworth-Heinemann, Oxford, pp 57–96. https://doi.org/10.1016/B978-1-85617-663-7.00004-7

Barthelat F, Li CM, Comi C, Espinosa HD (2006) Mechanical properties of nacre constituents and their impact on mechanical performance. J Mater Res 21(8):1977–1986. https://doi.org/10.1557/jmr.2006.0239

Barthelat F, Yin Z, Buehler MJ (2016) Structure and mechanics of interfaces in biological materials. Nat Rev Mater 1(4):16007. https://doi.org/10.1038/natrevmats.2016.7

Borodich FM, Bull SJ, Epshtein SA (2015) Nanoindentation in studying mechanical properties of heterogeneous materials. J Min Sci 51(3):470–476. https://doi.org/10.1134/S1062739115030072

Bouville F, Maire E, Meille S, Van de Moortèle B, Stevenson AJ, Deville S, de Moortèle B, Stevenson AJ, Deville S (2014) Strong, tough and stiff bioinspired ceramics from brittle constituents. Nat Mater 13(5):508–514. https://doi.org/10.1038/nmat3915

Briscoe BJ, Fiori L, Pelillo E (1998) Nano-indentation of polymeric surfaces. J Phys D Appl Phys 31(19):2395–2405. https://doi.org/10.1088/0022-3727/31/19/006

Bruet B, Qi H, Boyce M, Panas R, Tai K, Frick L, Ortiz C (2005) Nanoscale morphology and indentation of individual nacre tablets from the gastropod mollusc trochus niloticus. J Mater Res 20(9):2400–2419. https://doi.org/10.1557/jmr.2005.0273

Constantinides G, Ravi Chandran KS, Ulm FJ, Van Vliet KJ (2006) Grid indentation analysis of composite microstructure and mechanics: principles and validation. Mater Sci Eng A 430(1–2):189–202. https://doi.org/10.1016/j.msea.2006.05.125

Cook RF, Pharr GM (1990) Direct observation and analysis of indentation cracking in glasses and ceramics. J Am Ceram Soc 73(4):787–817. https://doi.org/10.1111/j.1151-2916.1990.tb05119.x

Dunlop JWC, Fratzl P (2010) Biological composites. Annu Rev Mater Res 40(1):1–24. https://doi.org/10.1146/annurev-matsci-070909-104421

Dunlop JWC, Weinkamer R, Fratzl P (2011) Artful interfaces within biological materials. Mater Today 14(3):70–78. https://doi.org/10.1016/S1369-7021(11)70056-6

Gao HL, Chen SM, Mao LB, Song ZQ, Yao HB, Cölfen H, Luo XS, Zhang F, Pan Z, Meng YF, Ni Y, Yu SH (2017) Mass production of bulk artificial nacre with excellent mechanical properties. Nat Commun 8(1):287. https://doi.org/10.1038/s41467-017-00392-z

George J, Sabapathi SN (2015) Cellulose nanocrystals: synthesis, functional properties, and applications. Nanotechnol Sci Appl 45. https://doi.org/10.2147/NSA.S64386

Gray D, Mu X (2015) Chiral nematic structure of cellulose nanocrystal suspensions and films; polarized light and atomic force microscopy. Materials 8(12):7873–7888. https://doi.org/10.3390/ma8115427

Gu GX, Libonati F, Wettermark SD, Buehler MJ (2017) Printing nature: unraveling the role of nacre's mineral bridges. J Mech Behav Biomed Mater 76:135–144. https://doi.org/10.1016/j.jmbbm.2017.05.007

Habibi Y, Lucia LA, Rojas OJ (2010) Cellulose nanocrystals: chemistry, self-assembly, and applications. Chem Rev 110(6):3479–3500. https://doi.org/10.1021/cr900339w

Hon DNS (1994) Cellulose: a random walk along its historical path. Cellulose 1(1):1–25. https://doi.org/10.1007/BF00818796

Imbeni V, Kruzic JJ, Marshall GW, Marshall SJ, Ritchie RO (2005) The dentin-enamel junction and the fracture of human teeth. Nat Mater 4(3):229–232. https://doi.org/10.1038/nmat1323

Jiang H, Browning R, Sue HJ (2009) Understanding of scratch-induced damage mechanisms in polymers. Polymer 50(16):4056–4065. https://doi.org/10.1016/j.polymer.2009.06.061

Khelifa F, Habibi Y, Bonnaud L, Dubois P (2016) Epoxy monomers cured by high cellulosic nanocrystal loading. ACS Appl Mater Interf 8(16):10535–10544. https://doi.org/10.1021/acsami.6b02013

Kim HJ, Park S, Kim SH, Kim JH, Yu H, Kim HJ, Yang YH, Kan E, Kim YH, Lee SH (2015) Biocompatible cellulose nanocrystals as supports to immobilize lipase. J Mol Catal B Enzym 122:170–178. https://doi.org/10.1016/j.molcatb.2015.09.007

Klemm D, Kramer F, Moritz S, Lindström T, Ankerfors M, Gray D, Dorris A (2011) Nanocelluloses: a new family of nature-based materials. Angew Chem Int Ed 50(24):5438–5466. https://doi.org/10.1002/anie.201001273

Kretschmann D (2003) Velcro mechanics in wood. Nat Mater 2(12):775–776. https://doi.org/10.1038/nmat1025

Kushch VI, Dub SN, Shmegera RS, Sirota YV, Tolmacheva GN (2015) Procedure of the multiple indentations for determination of the hardness parameters of structurally heterogeneous materials. J Superhard Mater 37(3):173–181. https://doi.org/10.3103/S1063457615030041

Lagerwall JPF, Schütz C, Salajkova M, Noh J, Hyun Park J, Scalia G, Bergström L (2014) Cellulose nanocrystal-based materials: from liquid crystal self-assembly and glass formation to multifunctional thin films. NPG Asia Mater 6(1):e80–e80. https://doi.org/10.1038/am.2013.69

Le Ferrand H, Bouville F, Niebel TP, Studart AR (2015) Magnetically assisted slip casting of bioinspired heterogeneous composites. Nat Mater 14(11):1172–1179. https://doi.org/10.1038/nmat4419

Li YQ, Yu T, Yang TY, Zheng LX, Liao K (2012) Bio-inspired nacre-like composite films based on graphene with superior mechanical, electrical, and biocompatible properties. Adv Mater 24(25):3426–3431. https://doi.org/10.1002/adma.201200452

Lichtenegger HC (2002) High Abrasion resistance with sparse mineralization: copper biomineral in worm jaws. Science 298(5592):389–392. https://doi.org/10.1126/science.1075433

Miller M, Bobko C, Vandamme M, Ulm FJ (2008) Surface roughness criteria for cement paste nanoindentation. Cem Concr Res 38(4):467–476. https://doi.org/10.1016/j.cemconres.2007.11.014

Moon RJ, Jakes JE, Beecher JF, Frihart CR, Stone DS (2009) Advanced biomass science and technology for bio-based products. In: Hse CY, Jiang Z, Kuo ML (eds) Relating nanoindentation to macroindentation of wood. Southern Research Station, Beijing, China, pp 145–159

Moon RJ, Martini A, Nairn J, Simonsen J, Youngblood J (2011) Cellulose nanomaterials review: structure, properties and nanocomposites. Chem Soc Rev 40(7):3941. https://doi.org/10.1039/c0cs00108b

Niebel TP, Bouville F, Kokkinis D, Studart AR (2016) Role of the polymer phase in the mechanics of nacre-like composites. J Mech Phys Solids 96:133–146. https://doi.org/10.1016/j.jmps.2016.06.011

Oliver WC, Pharr GM (1992) An improved technique for determining hardness and elastic modulus using load and displacement sensing indentation experiments. J Mater Res 7(06):1564–1583. https://doi.org/10.1557/JMR.1992.1564

Paplham WP, Seferis JC, BaltáCalleja FJ, Zachmann HG (1995) Microhardness of carbon fiber reinforced epoxy and thermoplastic polyimide composites. Polym Compos 16(5):424–428. https://doi.org/10.1002/pc.750160512

Pharr GM, Herbert EG, Gao Y (2010) The indentation size effect: a critical examination of experimental observations and mechanistic interpretations. Annu Rev Mater Res 40(1):271–292. https://doi.org/10.1146/annurev-matsci-070909-104456

Pro JW, Barthelat F (2019) The fracture mechanics of biological and bioinspired materials. MRS Bull 44(1):46–52. https://doi.org/10.1557/mrs.2018.324

Pruksawan S, Samitsu S, Fujii Y, Torikai N, Naito M (2020) Toughening effect of rodlike cellulose nanocrystals in epoxy adhesive. ACS Appl Polymer Mater 2(3):1234–1243. https://doi.org/10.1021/acsapm.9b01102

Randall NX, Vandamme M, Ulm FJ (2009) Nanoindentation analysis as a two-dimensional tool for mapping the mechanical properties of complex surfaces. J Mater Res 24(03):679–690. https://doi.org/10.1557/jmr.2009.0149

Rao A, Divoux T, McKinley GH, Hart AJ (2019) Shear melting and recovery of crosslinkable cellulose nanocrystal-

polymer gels. Soft Matter 15(21):4401–4412. https://doi.org/10.1039/C8SM02647E

Ritchie RO (2011) The conflicts between strength and toughness. Nat Mater 10(11):817–822. https://doi.org/10.1038/nmat3115

Schütz C, Agthe M, Fall AB, Gordeyeva K, Guccini V, Salajková M, Plivelic TS, Lagerwall JPF, Salazar-Alvarez G, Bergström L (2015) Rod packing in chiral nematic cellulose nanocrystal dispersions studied by small-angle x-ray scattering and laser diffraction. Langmuir 31(23):6507–6513. https://doi.org/10.1021/acs.langmuir.5b00924

Shell De Guzman M, Neubauer G, Flinn P, Nix WD (1993) The role of indentation depth on the measured hardness of materials. MRS Proc 308:613. https://doi.org/10.1557/PROC-308-613

Shen L, Phang IY, Liu T, Zeng K (2004) Nanoindentation and morphological studies on nylon 66/organoclay nanocomposites. II. Effect of strain rate. Polymer 45(24):8221–8229. https://doi.org/10.1016/j.polymer.2004.09.062

Siqueira G, Kokkinis D, Libanori R, Hausmann MK, Gladman AS, Neels A, Tingaut P, Zimmermann T, Lewis JA, Studart AR (2017) Cellulose nanocrystal inks for 3d printing of textured cellular architectures. Adv Funct Mater 1604619. https://doi.org/10.1002/adfm.201604619

Skrzypczak M, Guerret-Piecourt C, Bec S, Loubet JL, Guerret O (2009) Use of a nanoindentation fatigue test to characterize the ductile-brittle transition. J Eur Ceram Soc 29(6):1021–1028. https://doi.org/10.1016/j.jeurceramsoc.2008.07.066

Song J, Fan C, Ma H, Wei Y (2015) Hierarchical structure observation and nanoindentation size effect characterization for a limnetic shell. Acta Mech Sin 31(3):364–372. https://doi.org/10.1007/s10409-015-0405-x

Song J, Chen C, Zhu S, Zhu M, Dai J, Ray U, Li YY, Kuang Y, Li YY, Quispe N, Yao Y, Gong A, Leiste UH, Bruck HA, Zhu JY, Vellore A, Li H, Minus ML, Jia Z, Martini A, Li T, Hu L (2018) Processing bulk natural wood into a high-performance structural material. Nature 554(7691):224–228. https://doi.org/10.1038/nature25476

Staines M, Robinson WH, Hood JAA (1981) Spherical indentation of tooth enamel. J Mater Sci 16(9):2551–2556. https://doi.org/10.1007/BF01113595

Tesch W, Eidelman N, Roschger P, Goldenberg F, Klaushofer K, Fratzl P (2001) Graded microstructure and mechanical properties of human crown dentin. Calcif Tissue Int 69(3):147–157. https://doi.org/10.1007/s00223-001-2012-z

Tze W, Wang S, Rials T, Pharr G, Kelley S (2007) Nanoindentation of wood cell walls: continuous stiffness and hardness measurements. Compos A Appl Sci Manuf 38(3):945–953. https://doi.org/10.1016/j.compositesa.2006.06.018

Wang J, Shaw LL (2009) Nanocrystalline hydroxyapatite with simultaneous enhancements in hardness and toughness. Biomaterials 30(34):6565–6572. https://doi.org/10.1016/j.biomaterials.2009.08.048

Wegst UGK, Bai H, Saiz E, Tomsia AP, Ritchie RO (2015) Bioinspired structural materials. Nat Mater 14(1):23–36. https://doi.org/10.1038/nmat4089

Zhao H, Kwak J, Conradzhang Z, Brown H, Arey B, Holladay J (2007) Studying cellulose fiber structure by SEM, XRD, NMR and acid hydrolysis. Carbohyd Polym 68(2):235–241. https://doi.org/10.1016/j.carbpol.2006.12.013

Zhao H, Yang Z, Guo L (2018) Nacre-inspired composites with different macroscopic dimensions: strategies for improved mechanical performance and applications. NPG Asia Mater 10(4):1–22. https://doi.org/10.1038/s41427-018-0009-6

Publisher's Note Springer Nature remains neutral with regard to jurisdictional claims in published maps and institutional affiliations.